



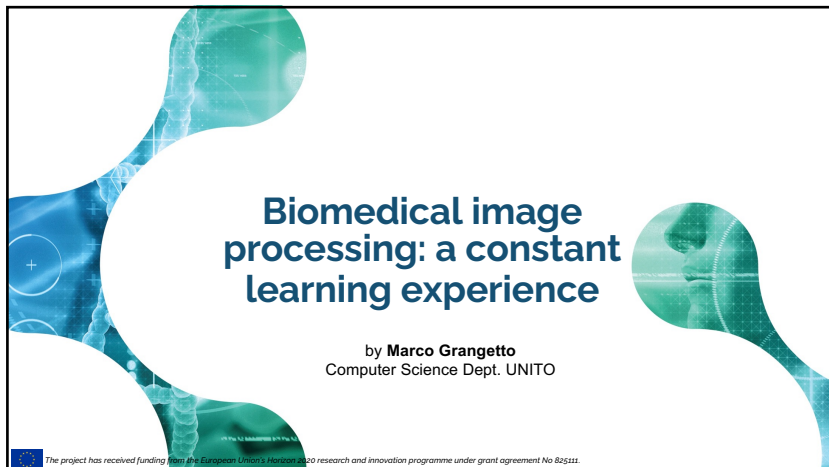
1

The slide has a blue and white abstract background with a brain scan. At the top right is the DEEPHEALTH logo. Below it, the word "Outline" is written. A bulleted list follows:

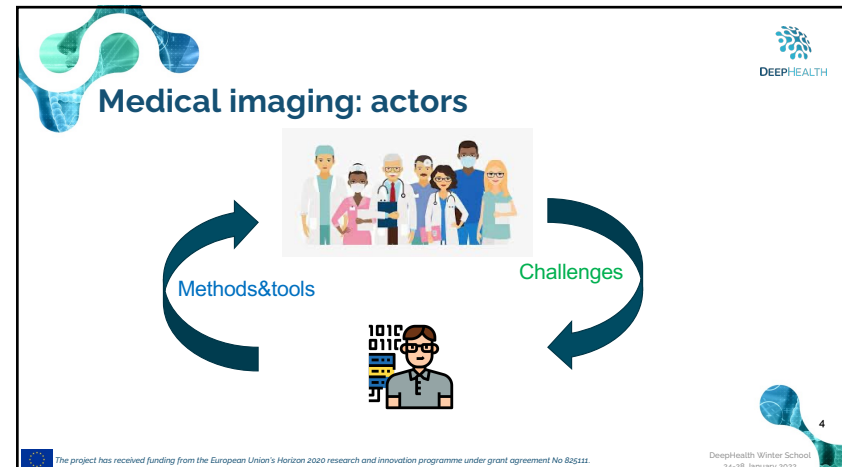
- Introduction to medical imaging: a constant learning experience (**Marco Grangetto**)
- From H&E to pixels: digital pathology applications for colon cancer diagnosis (**Luca Bertero, Carlo Barbano**)
- Lung cancer diagnosis (**Daniele Perlo, Riccardo Renzulli, Marco Grosso**)
- Neural Network-derived perfusion maps in patients with acute ischemic stroke (**Federico D'Agata, Enzo Tartaglione**)

At the bottom left is the European Union funding logo, and at the bottom right is the text "DeepHealth Winter School 24-28 January 2022".

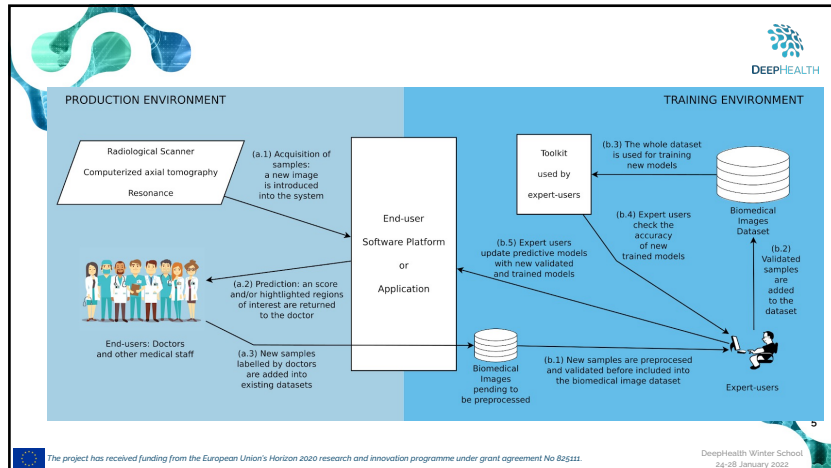
2



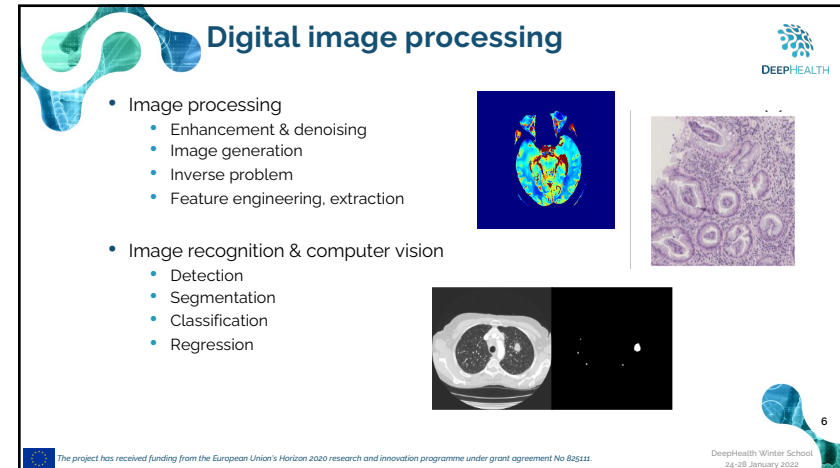
3



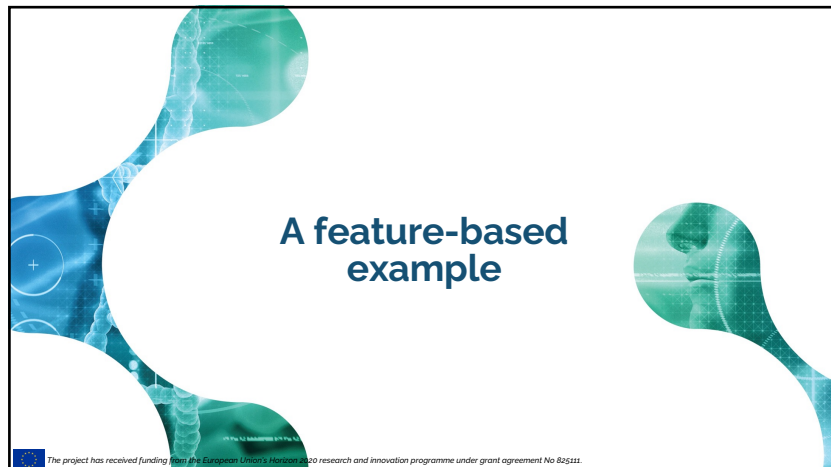
4



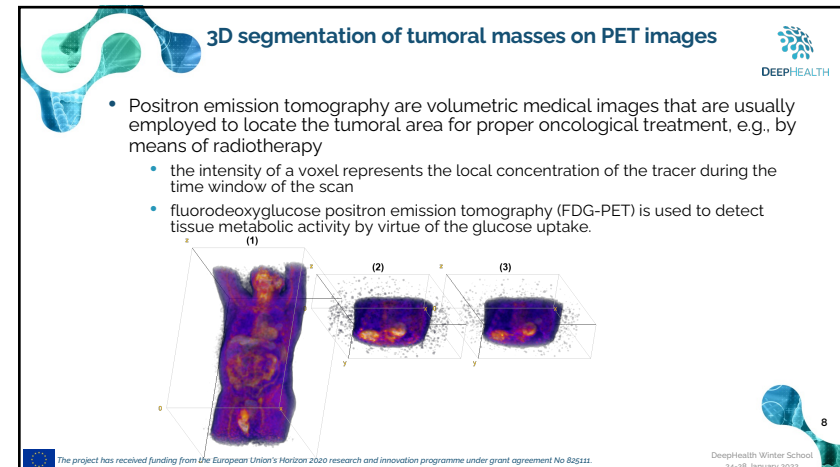
5



6



7



8

**3D segmentation of tumoral masses on PET images**

DEEPHEALTH

- Challenge: segmentation of cells with abnormal metabolism
  - Problem understanding, small data collection
- Methods: Anomaly detection
  - Method identification
- Tools: Reed-Xiaoli detector (RXD), statistical detector based on temporal/spatial correlation
  - Feature engineering/extraction -> detection
- Experimental validation
  - metric definition

	Average
RXD	0.570
LAD ( $I_Q$ )	0.362
LAD-S ( $I_Q$ )	<b>0.592</b>
LAD ( $I_C$ )	0.427
LAD-S ( $I_C$ )	0.560

F. Verdoja, M. Grangetto. "Graph Laplacian for image anomaly detection." *Machine Vision and Applications* 31.1 (2020): 1-16

The project has received funding from the European Union's Horizon 2020 research and innovation programme under grant agreement No 825111.

DeepHealth Winter School  
24-28 January 2022

9

**Feature-based approach**

DEEPHEALTH

### Challenge

Data samples

- Problem understanding and method mapping
- Tool/model selection based on target features
- Development and validation

The project has received funding from the European Union's Horizon 2020 research and innovation programme under grant agreement No 825111.

DeepHealth Winter School  
24-28 January 2022

11

**A deep-learning example**

The project has received funding from the European Union's Horizon 2020 research and innovation programme under grant agreement No 825111.

DeepHealth Winter School  
24-28 January 2022

12

**Covid-diagnosis from CXR**

DEEPHEALTH

A learning based example

Encoder

Hierarchical Classifier

FC1

FC2

cov=1 pred=0.92

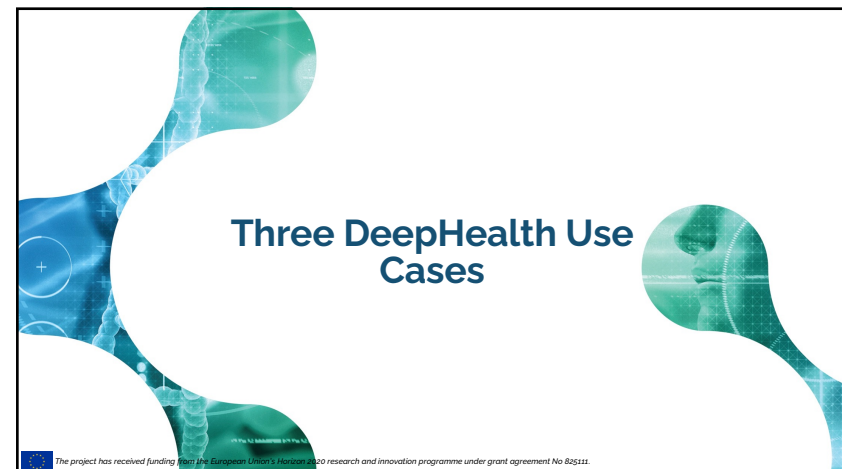
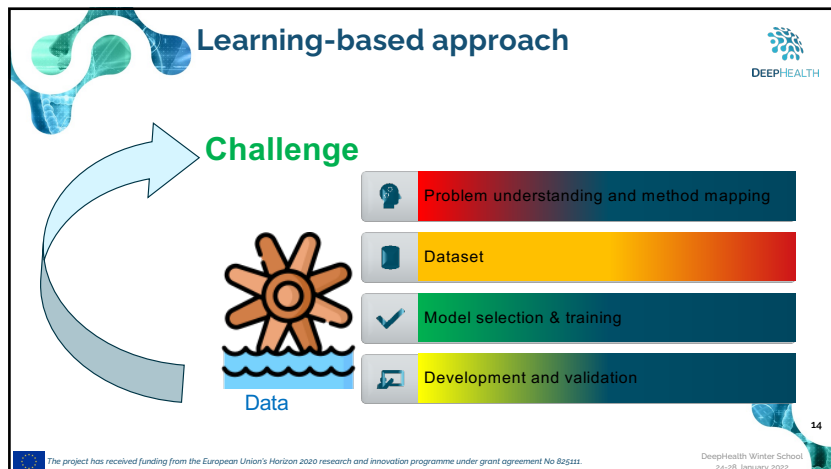
cov=1 pred=0.93

Tartaglione, Enzo, et al. "Unveiling covid-19 from chest x-ray with deep learning: a hurdles race with small data." *International Journal of Environmental Research and Public Health* 17.18 (2020)

The project has received funding from the European Union's Horizon 2020 research and innovation programme under grant agreement No 825111.

DeepHealth Winter School  
24-28 January 2022

13



UNIVERSITÀ DEGLI STUDI DI TORINO

ASISTENZA OSPEDALIERA UNIVERSITARIA Città della Salute e della Scienza di Torino

(b) HP

(a) HG

**From H&E to pixels: digital pathology applications for colon cancer diagnosis**

L. BERTERO

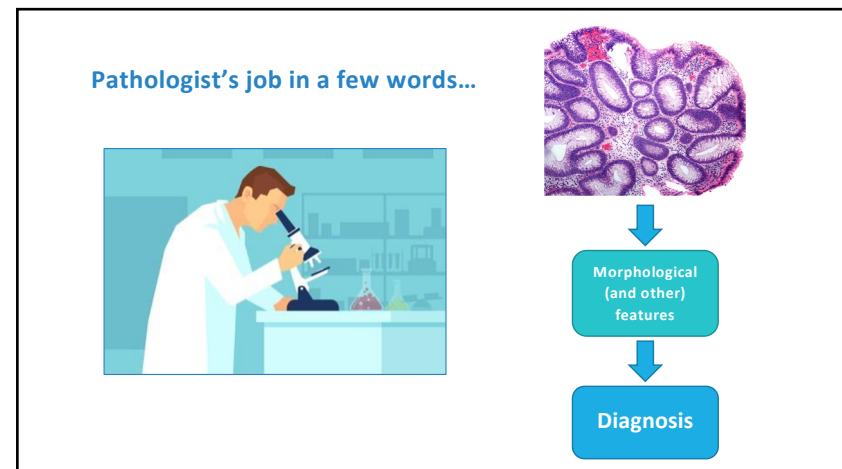
Div. of Pathology, Dept. Medical Sciences  
University of Turin, Italy

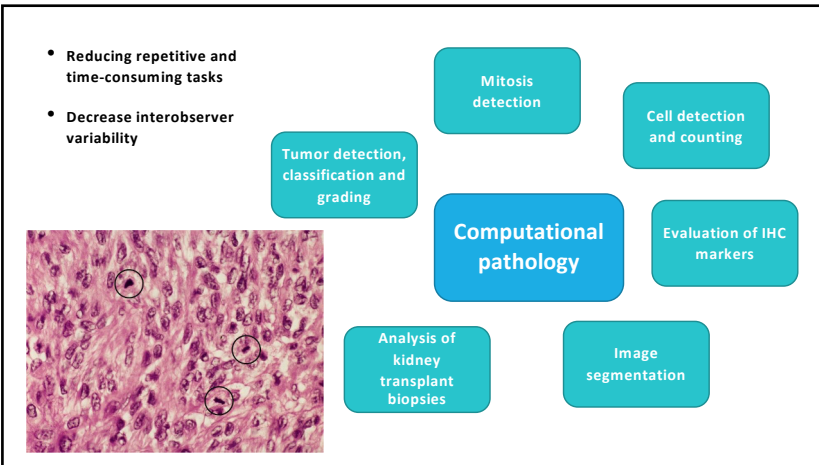
C. A. BARBANO

Computer Science dept.  
University of Turin, Italy

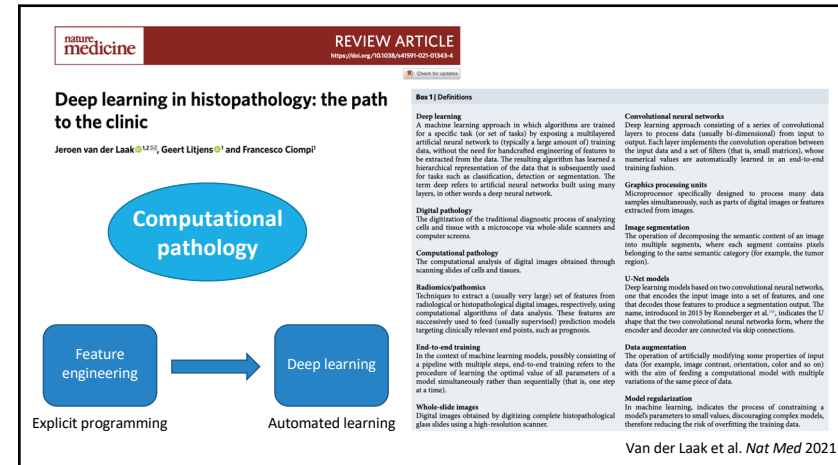
The project has received funding from the European Union's Horizon 2020 research and innovation programme under grant agreement No 825111.

16

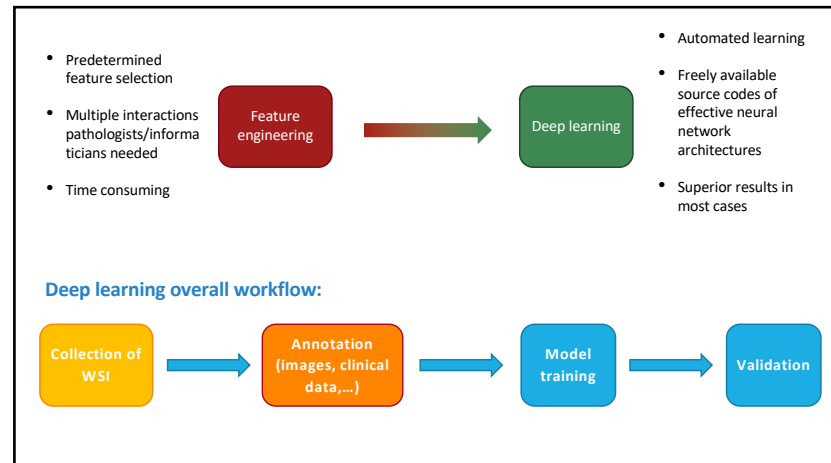




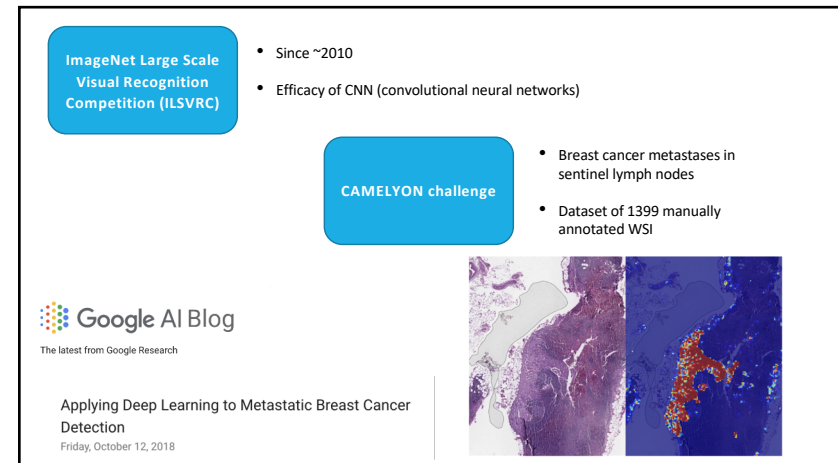
18



19



20



21

**Colon cancer diagnosis**

Colon cancer is one of the most frequent causes of death. Screening programs can enable prompt diagnosis and treatment of this aggressive disease, but they also lead to higher caseloads and costs for the already strained European healthcare services. DeepHealth can help streamline pathological diagnosis of colon biopsies.

**Use Cases**  
14 pilot test-beds in 3 areas:

- Neurological diseases
  - Migraine and Seizures prediction
  - Major Depression
  - Dementia
  - Study of structural changes in lumbar spine pathology
  - Population model for Alzheimer's Disease
  - Epileptic seizures detection
  - Objective fatigue assessment for multiple sclerosis patients
- Tumor detection and early cancer prediction
  - Chest cancer detection
  - Prostate tumor diagnosis
  - Skin cancer melanoma detection
  - Digital pathology and automated image annotation
- Classification of whole-slide histological analysis of colorectal biopsy samples
  - CT brain perfusion maps synthesis
  - Deep Image annotation
  - Image Analysis and prediction for Urology

22

## Colorectal carcinoma

Number of deaths in 2020, both sexes, all ages

Cancer Type	Number of Deaths (2020)	Percentage
Lung	1,796,144	18%
Other cancers	3,557,464	35.7%
Colorectum	935,173	9.4%
Prostate	375,304	3.8%
Pancreas	466,003	4.7%
Liver	830,180	8.3%
Stomach	768,793	7.7%
Oesophagus	544,076	5.5%
Breast	684,996	6.9%
Total	9,958,133	

• Colorectal carcinoma (CRC) is the **second most deadly** and the **third most common cancer** (Globocan 2020)

• Colorectal cancer screening enables prompt detection of early CRC or preinvasive lesions, but represents a significant workload for both **endoscopy** and **pathology** units

23

## Digital pathology for colorectal neoplasms

- Distinction between tumor tissue and stroma (Kather JN et al. *Sci Rep* 2016)
- Outcome prediction (Bychkov D et al. *Sci Rep* 2018; Kather JN et al. *PLoS Med* 2019; Skrede O et al. *Lancet* 2020)
- Molecular profile prediction (Yamashita R et al., *Lancet Oncol* 2020; Sirinukunwattana K et al. *Gut* 2021; Bilal M et al. *Lancet Digit Health* 2021)
- Polyps detection and classification...

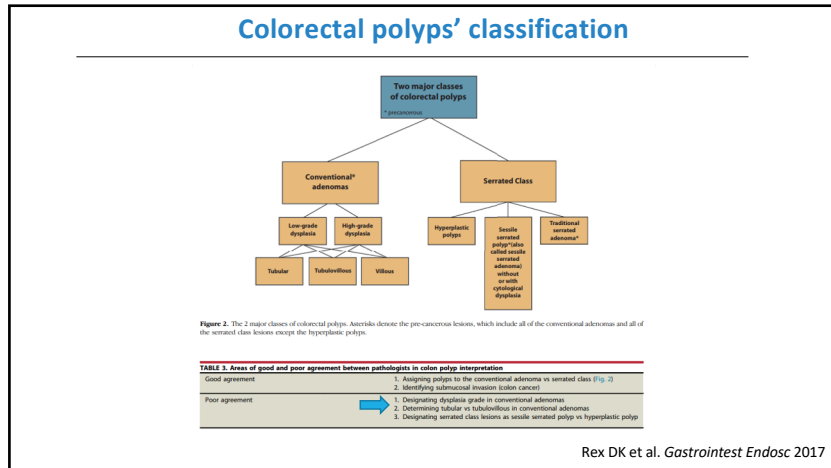
24

## Colorectal polyps

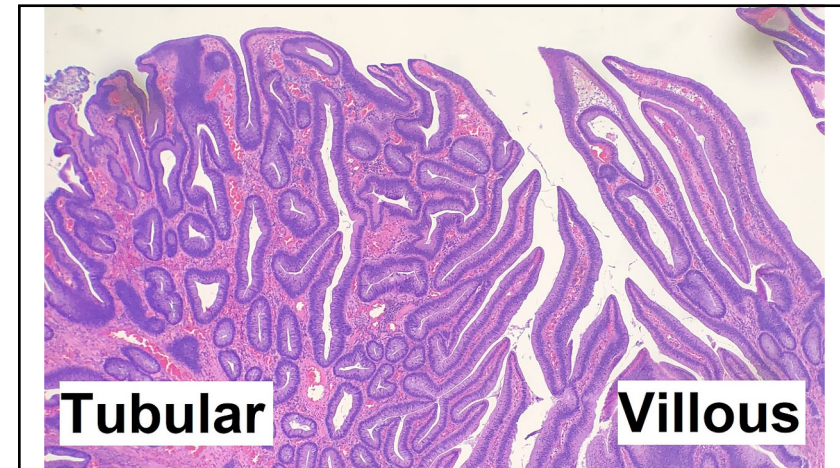
- The vast majority of colorectal carcinomas (CRC) arises from  **premalignant polyps**, usually in a process that take many years
- Premalignant polyps are **very frequent**, occurring in a quarter to a half of population >50 years
- However, only about 5% of the population will ultimately develop an invasive CRC and some features have been identified to predict the risk of invasive CRC, including polyp histopathological type

- Colorectal polyps are a significant workload for endoscopy and pathology units worldwide
- Correct histopathological classification of colorectal polyps is critical to tailor the following management

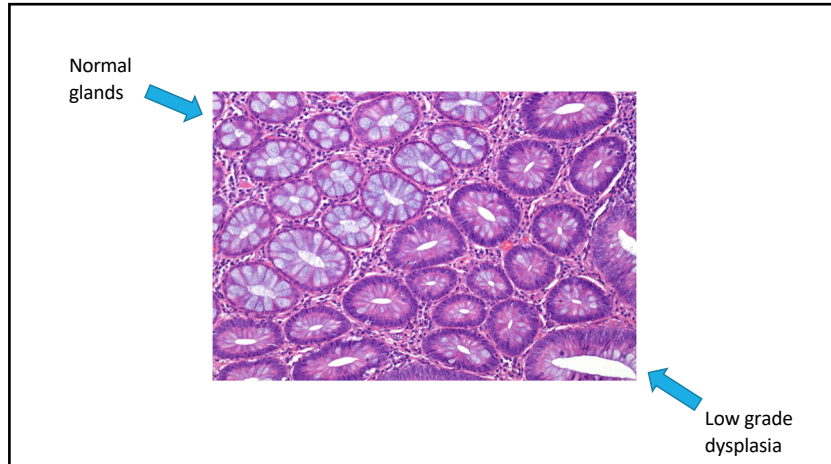
25



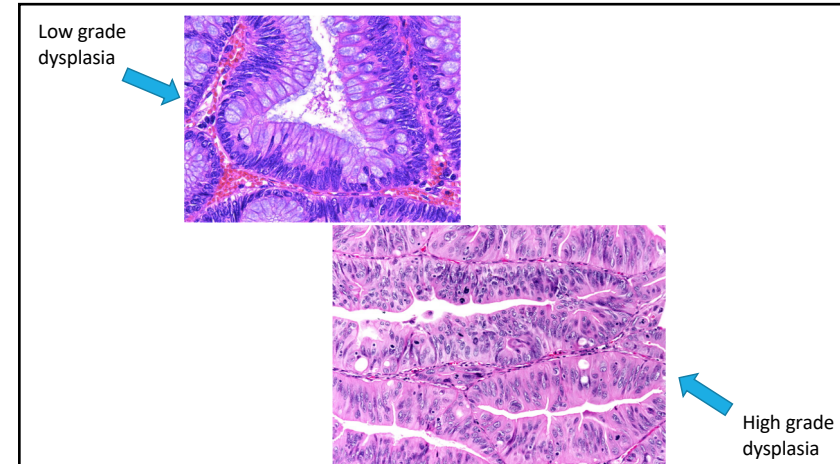
26



27



28



29

**Why does it matter?**

**Post-polypectomy colonoscopy surveillance: European Society of Gastrointestinal Endoscopy (ESGE) Guideline – Update 2020**

**Authors:** Cesare Hasson<sup>1</sup>, Giulio Antonelli<sup>1</sup>, Jean-Marc Dumonceau<sup>1</sup>, Jarodlaw Regula<sup>2</sup>, Michael Bretthauer<sup>3</sup>, Stanislas Chassade<sup>2</sup>, Eveline Dekker<sup>4</sup>, Monika Ferlicits<sup>5</sup>, Antonio Gimeno-Garcia<sup>6</sup>, Rodrigo Jover<sup>7</sup>, Mette Kalager<sup>8</sup>, Mario Pelizzetti<sup>9</sup>, Christian Pox<sup>10</sup>, Luigi Ricciardelli<sup>11</sup>, Matthew Rutter<sup>12</sup>, Use Marklund Helsingør<sup>13</sup>, Arne Bleijenberg<sup>14</sup>, Carlo Senatore<sup>15</sup>, Jeanne E. van Heuvel<sup>16</sup>, Mario Driss-Ribeiro<sup>17</sup>, Enrique Quintela<sup>18</sup>

**• Polyp requiring surveillance:**

- 1 adenoma  $\geq 10$  mm
- High grade dysplasia**
- $\geq 5$  adenomas
- Any serrated polyp  $\geq 10$ mm or with dysplasia

```

graph TD
    A[High quality colonoscopy] --> B{Polyp requiring surveillance?}
    B -- Yes --> C[3-year surveillance]
    B -- No --> D[Return to screening]
    C --> E{Polyp requiring surveillance?}
    E -- Yes --> F[5-year surveillance]
    E -- No --> D
    F --> G{Polyp requiring surveillance?}
    G -- Yes --> H[Return to screening]
    G -- No --> D
  
```

30

**Real-time detection of colon polyps during colonoscopy using deep learning: systematic validation with four independent datasets**

Ji Young Lee<sup>1,2</sup>, Jinhoon Jeong<sup>2,3</sup>, Eun Mi Song<sup>2</sup>, Chunae Ha<sup>3</sup>, Hyo Jeong Lee<sup>4</sup>, Ja Eun Koo<sup>5</sup>, Dong-Hoon Yang<sup>6</sup>, Namkug Kim<sup>2,3,7</sup> & Jeong-Sik Byeon<sup>2,3,8</sup>

SCIENTIFIC REPORTS | (2020) 10:8379 | https://doi.org/10.1038/s41598-020-65387-1

**Accuracy of artificial intelligence on histology prediction and detection of colorectal polyps: a systematic review and meta-analysis**

Thomas K. L. Lui, MBBS, Chuan-Guo Guo, MMed, Wai K. Leung, MD

Volume 92, No. 1 : 2020 GASTROINTESTINAL ENDOSCOPY 11

31

**Adenoma classification**

**Deep Learning for Classification of Colorectal Polyps on Whole-slide Images**

Bruno Korbar<sup>1,2</sup>, Andrea M. Olstson<sup>2</sup>, Allen P. Miralbell<sup>2</sup>, Catherine M. Nick<sup>2</sup>, Matthew A. Suriawinata<sup>3</sup>, Lorenzo Torresani<sup>2</sup>, Arief A. Suriawinata<sup>2</sup>, Saeed Hassanzadeh<sup>1,2,4</sup>

*J Pathol Inform* 2017, 1:30

**Table 1: Our dataset: The distribution of colorectal polyp types in crop images used in this work**

Colorectal polyp type	Acronym	Number of image crops
Hyperplastic polyp	HP	205
Sessile serrated polyp	SSP	612
Traditional serrated adenoma	TSA	258
Tubular adenoma	TA	360
Tubulovillous/villous adenoma	TVA/V	202
Normal	-	237
Total	-	2074

**Table 4: Whole-slide classification results: Results of our final model for classification of colorectal polyps on 239 whole-slide images in our test set**

	HP (n=37) (%)	SSP (n=39) (%)	TSA (n=38) (%)	TA (n=39) (%)	TVA/V (n=38) (%)	Normal (n=48) (%)	Total (n=239) (%)
Accuracy	89.8 (85.3-94.3)	89.5 (85.0-93.1)	94.7 (91.1-97.2)	93.1 (89.2-96.0)	95.8 (92.5-97.9)	95.0 (91.5-97.4)	93.0 (89.0-95.9)
Precision	90.9 (86.6-94.2)	86.11 (81.1-90.2)	100.0 (98.5-100)	83.3 (78.0-87.8)	97.2 (94.3-98.9)	80.7 (75.1-85.5)	89.7 (85.2-93.2)
Recall	81.1 (75.5-85.8)	81.6 (76.1-86.3)	89.5 (84.9-93.0)	89.7 (85.2-93.3)	92.1 (88.0-95.2)	95.8 (92.5-98.0)	88.3 (83.6-92.1)
F1 score	85.7 (80.6-89.9)	83.8 (78.5-88.2)	94.4 (90.8-97.0)	86.4 (81.4-90.5)	94.6 (90.9-97.1)	87.6 (82.8-91.5)	88.8 (84.1-92.5)

HP: Hyperplastic polyp; SSP: Sessile serrated polyp, TSA: Traditional serrated adenoma, TA: Tubular adenoma, TVA/V: Tubulovillous/villous adenoma

32

**Adenoma classification**

**JAMA Network Open**

**Original Investigation | Health Informatics**

**Evaluation of a Deep Neural Network for Automated Classification of Colorectal Polyps on Histopathologic Slides**

Jason W. Wei, BA; Arif A. Suriawinata, MD; Louis J. Vachas, MD, PhD; Bing Ren, MD, PhD; Xuying Liu, MD; Mikhail Lisovskiy, MD, PhD; Naofumi Tomita, MS; Behnaz Abdollahi, PhD; Adam S. Kim, MD; Dale C. Snover, MD; John A. Baron, MD; Elizabeth L. Barry, PhD; Saeed Hassanzadeh, PhD

*JAMA Network Open*. 2020;3(4):e203398. doi:10.1001/jamanetworkopen.2020.3398

**Figure 1. Data Flow Diagram for the Study**

**Training set slides:**

- 37 Tubular
- 30 Tubulovillous or villous
- 111 Hyperplastic
- 113 Sessile serrated
- 8 Normal
- 326 Total

**Pathologist annotation:**

- 397 Tubulovillous or villous
- 1597 Hyperplastic
- 1137 Normal
- 3848 Total

**Training set cropped images:**

- 147 Tubular
- 91 Tubulovillous or villous
- 41 Hyperplastic
- 113 Normal
- 238 Total

**Validation set slides:**

- 5 Tubular
- 3 Tubulovillous or villous
- 1 Hyperplastic
- 5 Sessile serrated
- 25 Total

**Validation set patches:**

- 90 Tubular
- 91 Tubulovillous or villous
- 16 Hyperplastic
- 16 Sessile serrated
- 233 Normal
- 699 Total

**External test set:**

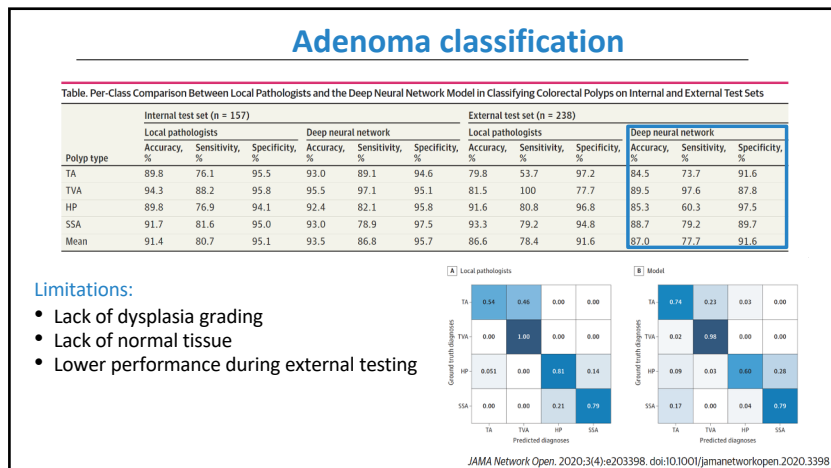
- 93 Tubular
- 78 Tubulovillous or villous
- 41 Hyperplastic
- 100 Normal
- 238 Total

**Internal test set:**

- 46 Tubular
- 34 Tubulovillous or villous
- 10 Hyperplastic
- 38 Sessile serrated
- 157 Total

**Performance analysis and comparison with local pathologists**

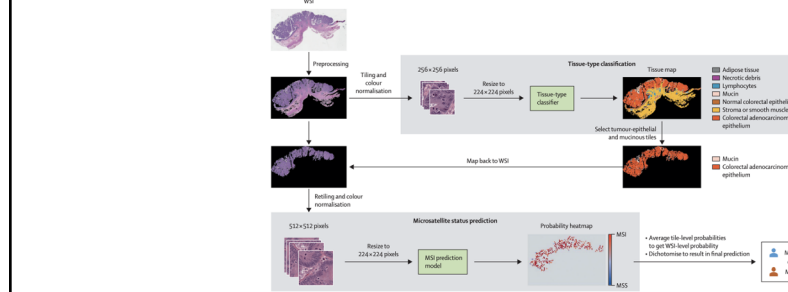
33



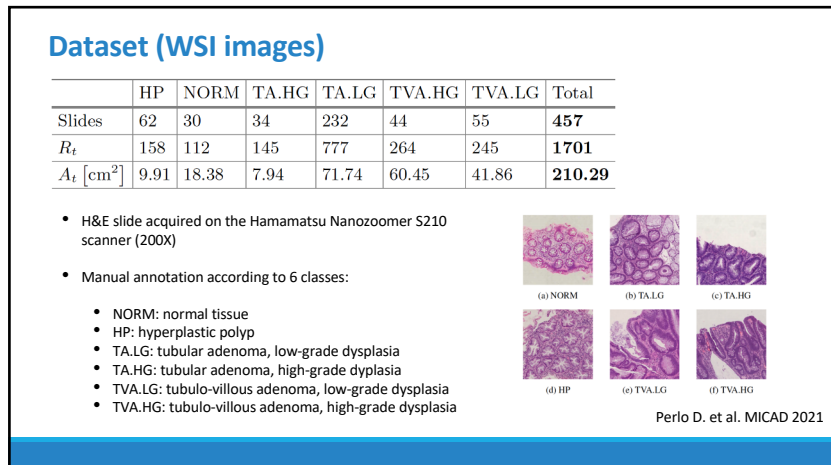
34

## Deep learning model for the prediction of microsatellite instability in colorectal cancer: a diagnostic study

Rikiya Yamashita, Jin Long, Teri Longacre, Lan Peng, Gerald Berry, Brock Martin, John Higgins, Daniel L Rubin\*, Jeanne Shen\*

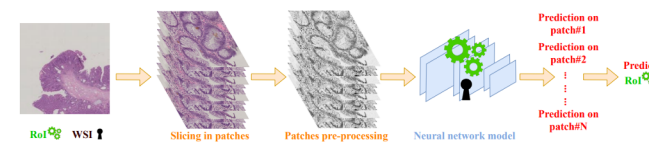
*Lancet Oncol* 2020; 22: 132-41

35



36

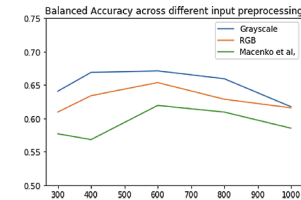
## Classification

Input images are **LARGE** -> Cannot process entire image at once

Perlo D. et al. MICAD 2021

37

- CNN: ResNet-18
- Pre-training on the ImageNet classification task
- Data augmentation: one random operation between rotation, equalization, solarization, inversion and contrast enhancing



**Patches normalization:** relevant features are not embed in color, but in image texture and signal strength

Fig. 2. Patches classification performance.

Perlo D. et al. MICAD 2021

38

### Patches resolution:

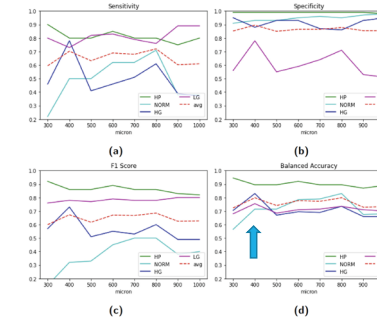


Table 3. Human dysplasia diagnostic performance comparison

	Accuracy	Sensitivity	Specificity
Hyperplastic	Our (400 $\mu\text{m}$ ) 0.90	0.80	<b>0.99</b>
	Our (600 $\mu\text{m}$ ) <b>0.92</b>	<b>0.85</b>	0.99
	Pathologist [8] 0.79	0.30	0.97
Low grade	Our (400 $\mu\text{m}$ ) <b>0.76</b>	0.73	<b>0.78</b>
	Our (600 $\mu\text{m}$ ) 0.71	<b>0.83</b>	0.59
High grade	Our (400 $\mu\text{m}$ ) <b>0.83</b>	0.78	0.88
	Our (600 $\mu\text{m}$ ) 0.70	0.46	<b>0.93</b>
	Pathologist [8] <b>0.83</b>	<b>0.81</b>	0.84

- Achieved results are similar to those reported by Denis B et al. (Eur J of Gastroenterol Hepatol 2009)

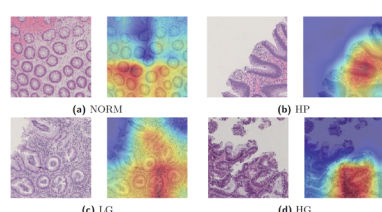
Perlo D. et al. MICAD 2021

39

### Dysplasia grading

Table 4. WSI inferences: confusion matrices.

		Predicted			
		HP	NORM	HG	LG
Gr. truth	HP	<b>0.85</b>	0	0.05	0.1
	NORM	0.12	<b>0.75</b>	0	0.12
Gr. truth	HG	0.02	0	<b>0.63</b>	0.35
	LG	0.03	0.09	0.18	<b>0.7</b>



- Poor results in distinguishing TA versus TVA/VA



Perlo D et al. MICAD 2021

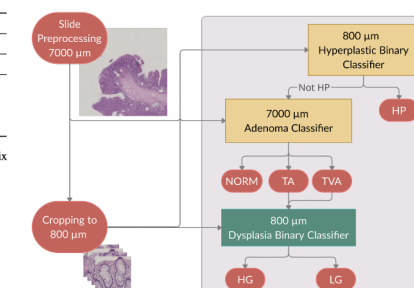
40

### Multi-resolution analysis

Type	100	800	1500	4000	7000	8000
BA (6-class)	0.40	0.45	<b>0.46</b>	0.41	0.37	0.38
NORM	0.70	0.66	0.72	0.76	0.78	0.71
HP	0.81	<b>0.92</b>	0.85	0.70	0.60	0.69
TA (HG+LG)	0.65	0.66	0.65	0.71	<b>0.76</b>	0.70
TVA (HG+LG)	0.64	0.67	0.68	0.74	<b>0.84</b>	0.76

Table 2: Preliminary experiments: overall BA for all of the six classes (first row) and BA for each polyp type, plus normal tissue.

- Adenoma type and dysplasia grade are best classified at different scales and resolutions



Barbano CA et al. IEEE ICIP 2021

41

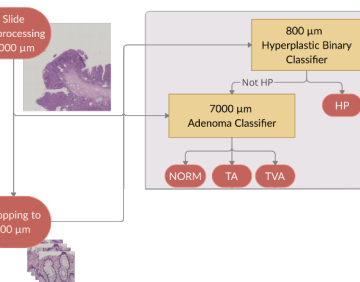
## Multi-resolution analysis

Type	100	800	1500	4000	7000	8000	Patch scale $\sigma$ [ $\mu\text{m}$ ]
BA (6-class)	0.40	0.45	<b>0.46</b>	0.41	0.37	0.38	
NORM	0.70	0.66	0.72	0.76	0.78	0.71	
HP	0.81	<b>0.92</b>	0.85	0.70	0.60	0.69	
TA (HG+LG)	0.65	0.66	0.65	0.71	<b>0.76</b>	0.70	
TVA (HG+LG)	0.64	0.67	0.68	0.74	<b>0.84</b>	0.76	

Table 2: Preliminary experiments: overall BA for all of the six classes (first row) and BA for each polyp type, plus normal tissue.

- HP is best determined with patches of 800x800 $\mu\text{m}$
- TA and TVA need larger areas of 7000x7000 $\mu\text{m}$
- Here, we can subsample patches to 224x224 pixels without any substantial loss in accuracy

Barbano CA et al. IEEE ICIP 2021



42

## Multi-resolution analysis

Type	100	800	1500	4000	7000	8000	Patch scale $\sigma$ [ $\mu\text{m}$ ]
BA (6-class)	0.40	0.45	<b>0.46</b>	0.41	0.37	0.38	
NORM	0.70	0.66	0.72	0.76	0.78	0.71	
HP	0.81	<b>0.92</b>	0.85	0.70	0.60	0.69	
TA (HG+LG)	0.65	0.66	0.65	0.71	<b>0.76</b>	0.70	
TVA (HG+LG)	0.64	0.67	0.68	0.74	<b>0.84</b>	0.76	

Table 2: Preliminary experiments: overall BA for all of the six classes (first row) and BA for each polyp type, plus normal tissue.

- Dysplasia grade is best determined with patches of 800 $\mu\text{m}$
- Here, we need to retain full-resolution images (no subsample) in order to prevent the loss of finer details such as cells nuclei

Barbano CA et al. IEEE ICIP 2021

43

## Multi-resolution analysis

HP	NORM	TA	TVA
HG	0.92	0.66	0.67
LG	0.87	0.92	0.92
BA	0.89	0.83	<b>0.81</b>

Table 3: Sensitivity, Specificity and BA per class.

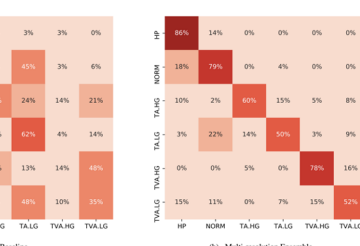
$\sigma$	HP	NORM	TA	TVA
Baseline	800	<b>0.92</b>	0.66	0.67
Baseline	1500	0.85	0.72	0.65
Baseline	7000	0.60	0.78	0.76
Multi-resolution	-	0.89	<b>0.83</b>	<b>0.81</b>

Table 4: Comparison of the class BA between the baseline and the proposed multi-resolution approach.

### Limitations:

- Some entities missing (serrated adenomas, invasive adenocarcinomas,...)
- Larger dataset is warranted
- Lack of external validation

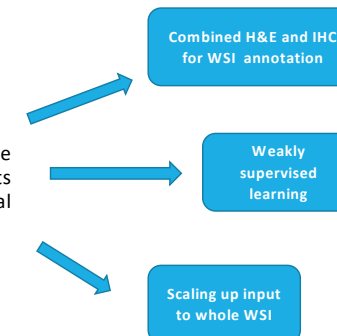
Barbano CA et al. IEEE ICIP 2021



44

## Challenges

- Collect large-scale annotated datasets (images and clinical annotations)



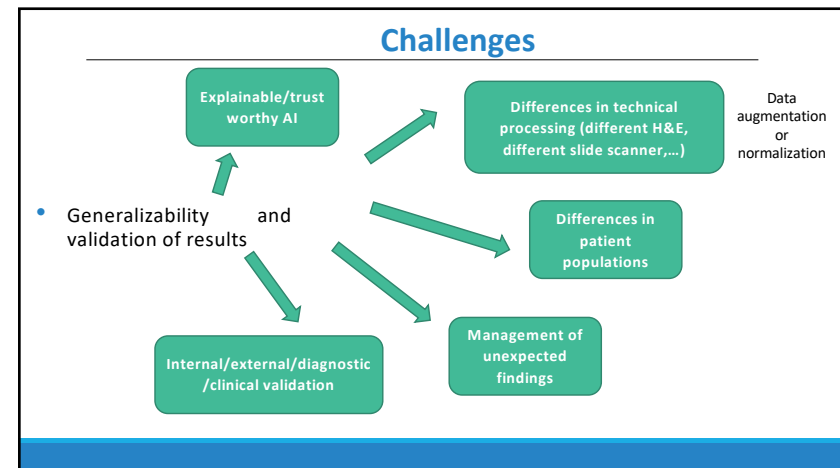
45

## GAN-Based data augmentation - WIP

Can you distinguish between ground truth and synthetized?

- GAN-based synthesis of new tissue patches to augment the existing data
- Using a C-GAN allows to target the generation for specific classes or dysplasia grade
- Using a semantic map as conditioning label allows for higher realism of the generated patch

46



47

## Lung cancer diagnosis

by Daniele Perlo (CDSS), Riccardo Renzulli (UNITO)  
Marco Grosso (CDSS)

The project has received funding from the European Union's Horizon 2020 research and innovation programme under grant agreement No 825111.

48



49



50

**Since 1703 for people's health**

Azienda Ospedaliero - Universitaria Città della Salute e della Scienza di Turin is an excellence multi-specialized organization integrated with the University of Turin Medical School. It provides clinical activities, on the basis of its 2200 hospital beds on a huge outpatients activity; teaching and research constitute a structural element of the Hospital, as well as of Italian National Health Service. The Hospital carries out many activities of research to develop innovative diagnostic and therapeutic procedures (e.g. it is the first in Europe in liver transplants).

The Radiology Department (Rad.Dept) of Azienda Ospedaliera Città della Salute e della Scienza di Torino is a great medical unit with about 100 Radiologists, 150 Radiographers, 10 Medical Physicists and a large support staff. Rad. Dept. includes radiological services of Molinette Hospital (large general hospital), Regina Margherita Hospital (pediatric), Sant'Anna Hospital (gynecological) and CTO Hospital (Trauma center). They have many teachers /researchers in: imaging, public health, social sciences, clinical governance, statistics, ICT, HTA and HIA. The department owns 1 Clinical MRI, PET-CT, 5 angiographic and interventional rooms and 1 Hybrid Radiology Unit. In addition, of course, to a wide range of radiological and ultrasound rooms.

It is a great research structure with more than 100 young physicians and radiographers in training.

It performs about 5000.000 imaging examinations at year.

The project has received funding from the European Union's Horizon 2020 research and innovation programme under grant agreement No 825111.

51



52

**DEEPHEALTH**

CT scan is a procedure that uses a computer linked to an x-ray machine to make a series of detailed pictures of areas inside the body. The pictures are taken from different angles and are used to create 3-dimensional (3-D) views of tissues and organs. A contrast media may be injected into a vein or swallowed to help the tissues and organs show up more clearly. A computed tomography scan may be used to help diagnose disease, plan treatment, or find out how well treatment is working. "Radiology 2" performs about 40.000 CT scans per year.

The project has received funding from the European Union's Horizon 2020 research and innovation programme under grant agreement No 825111.

53

**Pulmonary nodules**



Pulmonary nodules are small, focal, radiographic opacities that may be solitary or multiple.

A classic solitary pulmonary nodule (SPN) is a single, spherical, well-circumscribed, radiographic opacity measuring less than or equal to 30 mm in diameter and is surrounded completely by aerated lung. The SPN is a coined term that in the past described solitary nodules detected incidentally by chest radiography (CXR).

Today, most nodules are detected by computed tomography (CT). The detailed CT images frequently identify more than one nodule, or enlarged lymph nodes.

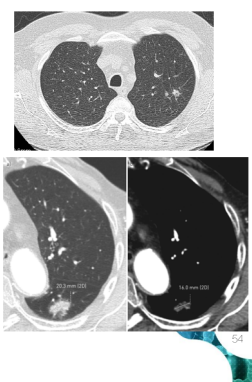
The term "solitary" should not be used in these circumstances. Indeterminate nodules are those that do not possess features clearly associated with a benign etiology, such as a benign pattern of calcification or stability on imaging for >2 years.

On CT scans, a nodule appears as a rounded or irregular opacity, well or poorly defined, measuring up to 3 cm in diameter.

Guidelines for Management of Incidental Pulmonary Nodules Detected on CT Images:  
From the Fleischner Society, 2017

 The project has received funding from the European Union's Horizon 2020 research and innovation programme under grant agreement No 825111

**DEEPHEALTH**



54

**Advances in chest imaging and the increased use of CT as a diagnostic modality**



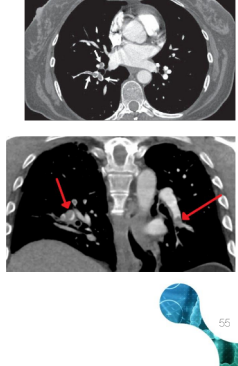
The lead to incidental identification of many small pulmonary nodules. The vast majority of nodules detected on CT are subcentimeter based on early lung screening trials (61%-89%).

The overwhelming majority of these are benign. The actual risk for malignancy in subcentimeter nodules is lower than the predicted risk based on clinical and radiographic criteria for pulmonary nodules. The Mayo Clinic CT Screening Trial reports 0% of nodules measuring <4 mm and 0.8% measuring between 4 and 7 mm in diameter are malignant. Another study reports 0% of nodules measuring <5 mm in diameter are malignant, while the rate is 5.9% of those measuring 5 to 9 mm in diameter.

NODULE DIMENSIONS	MALIGNANCY PROBABILITY
< 8 mm.	0.8 %
≤ 1 cm.	35 %
1 - 2 cm.	50 %
2 - 3 cm.	80 %
≥ 3 cm.	97 %

 The project has received funding from the European Union's Horizon 2020 research and innovation programme under grant agreement No 825111

**DEEPHEALTH**



55

**The prevalence of pulmonary nodules varies significantly across studies.**



This variation stems from the inconsistency among studies in method, enrolled population, and reporting results.

Most lung nodules are detected incidentally on CXR or CT scans obtained for other purposes. It is estimated that 0.09% to 0.2% of all CXR scans will incidentally detect pulmonary nodules.

In CT angiograms obtained to diagnose pulmonary embolism, a study reports 12% of cases to have incidental findings of pulmonary nodules.

In another cohort study, 31% of patients undergoing cardiac CT scans for coronary calcium scoring have incidental findings of pulmonary nodules.

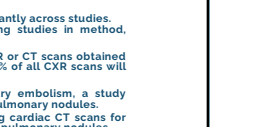
In lung cancer screening trials, 7% of CXR scans obtained from previously healthy individuals contain pulmonary nodules.

CT scans to screen for lung cancer detect nodules in 8% to 51% of individuals screened.

Benign	Malignant
Nonspecific granuloma (15%-25%)	Adenocarcinoma (47%)
Harmartoma (15%)	Squamous cell carcinoma (22%)
Infectious granuloma (15%)	
<ul style="list-style-type: none"> <li>Aspergillosis</li> <li>Coccidioidomycosis</li> <li>Cryptococcosis</li> <li>Histoplasmosis</li> <li>Tuberculosis</li> </ul>	<ul style="list-style-type: none"> <li>Metastatic (8%)</li> <li>Small cell lung carcinoma (4%)</li> </ul>
Others: lung abscess, round pneumonia, bronchogenic cysts, focal hemorrhage, hemangiomas, AVMs	Others: large cell carcinoma, carcinoid tumors, lymphomas, malignant teratomas

 The project has received funding from the European Union's Horizon 2020 research and innovation programme under grant agreement No 825111

**DEEPHEALTH**



56

**the task of the doctors was to identify, in the large archive of images (PACS), the cases that could be of interest to the computer scientists; we hope we have been good...**





 The project has received funding from the European Union's Horizon 2020 research and innovation programme under grant agreement No 825111

**DEEPHEALTH**



57

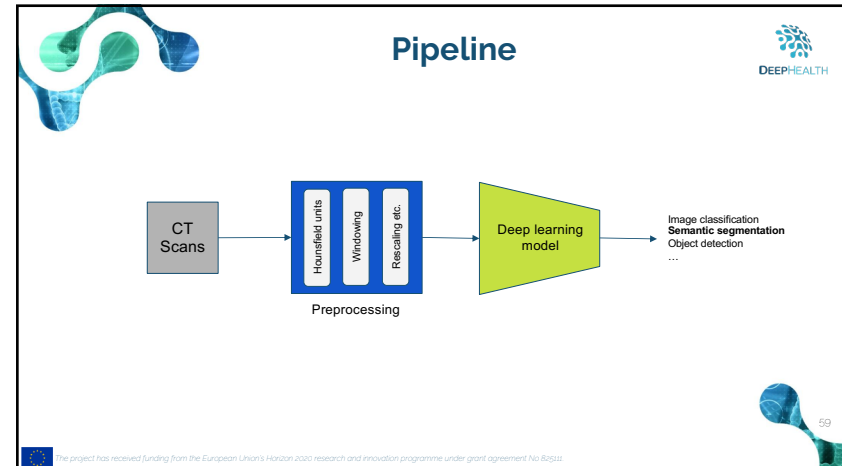
**Nodules segmentation**

Lung nodules are quite common incidental findings in CT (computed tomography) scans and can be defined as **small focal lesions** (ranging from 5 to 30 mm) that can be solitary or multiple.

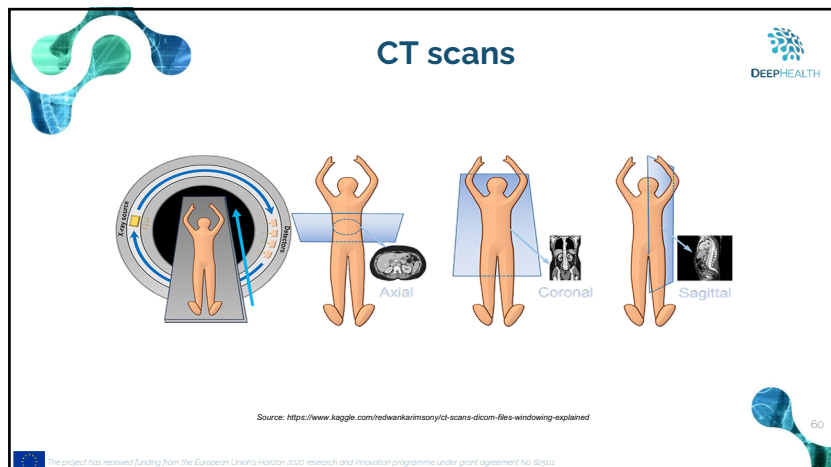
The goal of UC4 is to train **AI systems to recognize lung nodules** using chest CT scans, providing radiologists an efficient tool for daily activity.

The project has received funding from the European Union's Horizon 2020 research and innovation programme under grant agreement No 805111

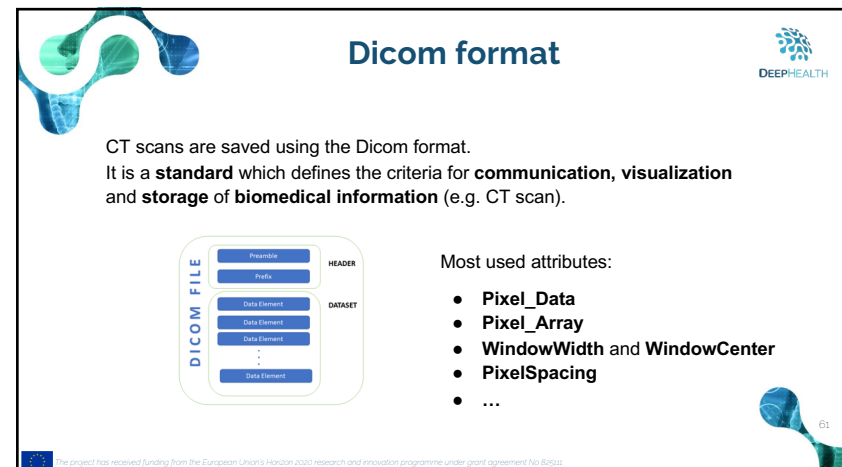
58



59



60

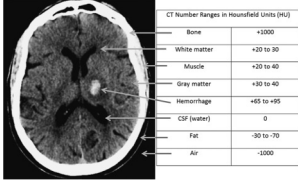


61

**Hounsfield units**

The DEEPHEALTH logo is in the top right corner.

First we need to converts raw pixel data values (provided by the attribute `Pixel_array`) to a specific (possibly unitless) physical quantity, such as **Hounsfield Units (HU)** for CT. It is a quantitative scale used for describing radiodensity.



CT Number Ranges in Hounsfield Units (HU)	
Bone	+1000
White matter	+20 to 30
Muscle	+20 to 40
Gray matter	+30 to 40
Hemorrhage	+65 to +95
CSF (water)	0
Fat	-30 to -70
Air	-1000

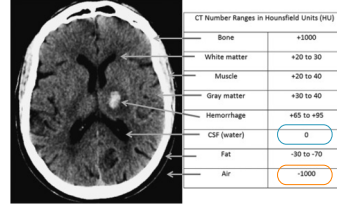
The project has received funding from the European Union's Horizon 2020 research and innovation programme under grant agreement No 805111.

62

**Hounsfield units**

The DEEPHEALTH logo is in the top right corner.

The HU scale is a linear transformation of the original linear attenuation coefficient measurement in one in which the radiodensity of **distilled water at standard pressure and temperature (STP)** is defined as **zero HU**, while the radiodensity of air at STP is defined as **-1000 HU**.



CT Number Ranges in Hounsfield Units (HU)	
Bone	+1000
White matter	+20 to 30
Muscle	+20 to 40
Gray matter	+30 to 40
Hemorrhage	+65 to +95
CSF (water)	0
Fat	-30 to -70
Air	-1000

It is a linear transformation  
 $y = (x * m) + b$ , where:

- $x$  is the stored **pixel value**.
- $m$  is the value of **Rescale Slope**.
- $b$  is the value of **Rescale Intercept**
- $y$  is the rescaled value (**HU**).

The project has received funding from the European Union's Horizon 2020 research and innovation programme under grant agreement No 805111.

63

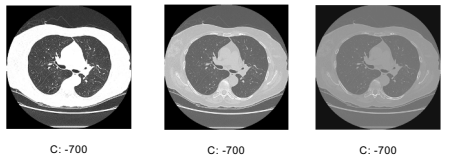
**Windowing operations**

The DEEPHEALTH logo is in the top right corner.

**WindowCenter (C) attribute (brightness)**



**WindowWidth (W) attribute (contrast)**



The project has received funding from the European Union's Horizon 2020 research and innovation programme under grant agreement No 805111.

64

**Windowing operations**

The DEEPHEALTH logo is in the top right corner.

Which windowing setting do we need to use?

↓

It depends on what you want to see!

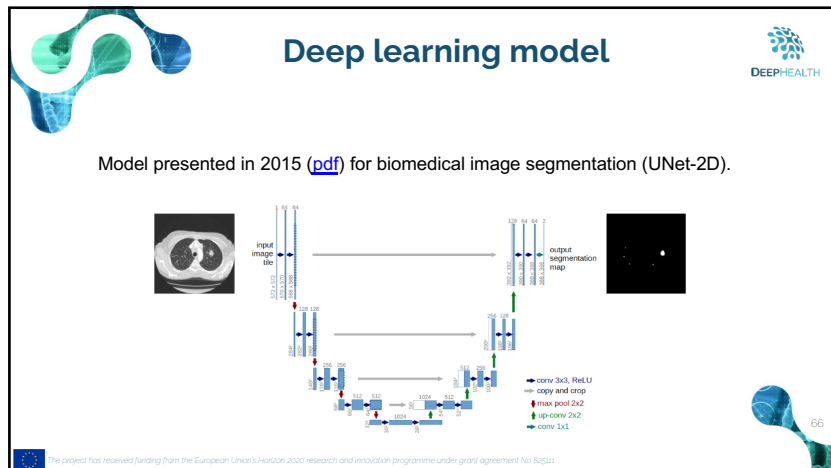
Lungs range C:-600 W:+1600

Mediastinum range C:+50 W:+500

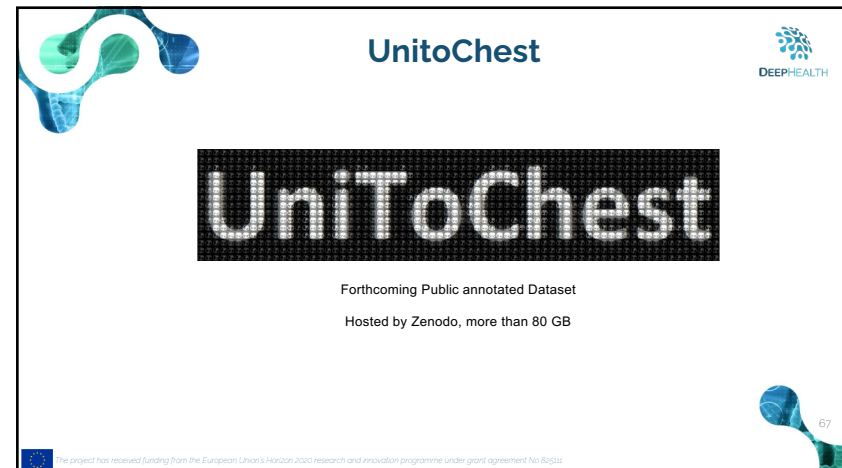
Bones range C:+400 W:+1800

The project has received funding from the European Union's Horizon 2020 research and innovation programme under grant agreement No 805111.

65



66



67

**UniToChest**

Dataset	Number of Patients	Number of Scans	Total Nodules count	Nodule Diameter range(mm)
LIDC – IDRI	1010	244527	7371	2 – 69
LUNA16	1010	888	1836	3 – 33
UniToChest	623	306440	11295	2 – 287

**Table 3. UniToChest vs others**

The project has received funding from the European Union's Horizon 2020 research and innovation programme under grant agreement No 80522.

DEEPHEALTH

68

**UniToChest**

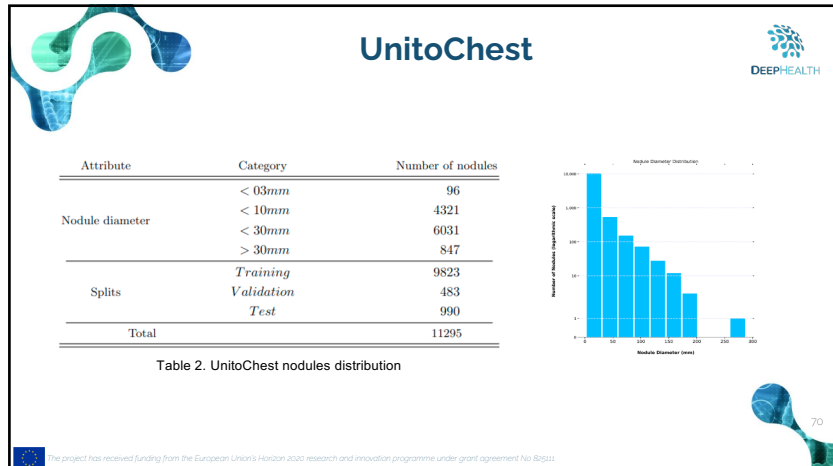
Dataset	Number of Patients	Number of Scans	Total Nodules count	Nodule Diameter range(mm)
LIDC – IDRI	1010	244527	7371	2 – 69
LUNA16	1010	888	1836	3 – 33
UniToChest	623	306440	11295	2 – 287

**Table 3. UniToChest vs others**

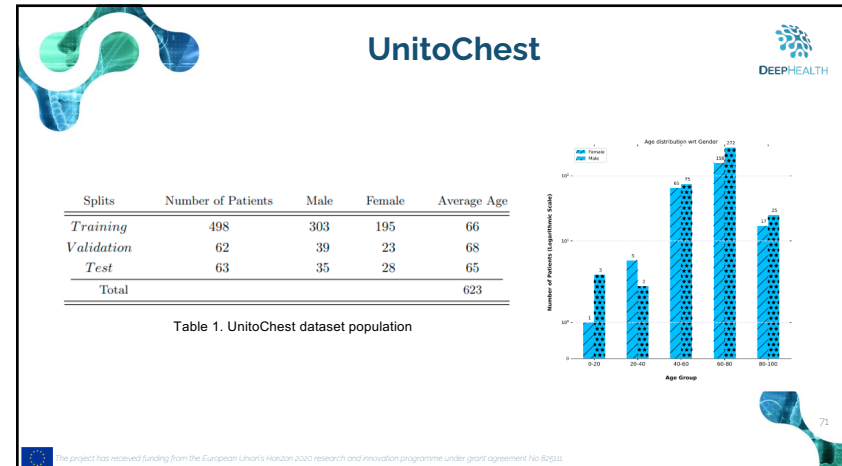
The project has received funding from the European Union's Horizon 2020 research and innovation programme under grant agreement No 80522.

DEEPHEALTH

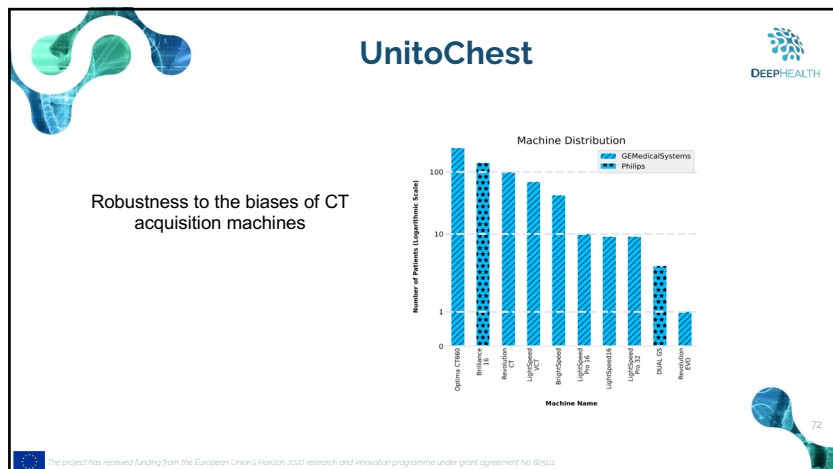
69



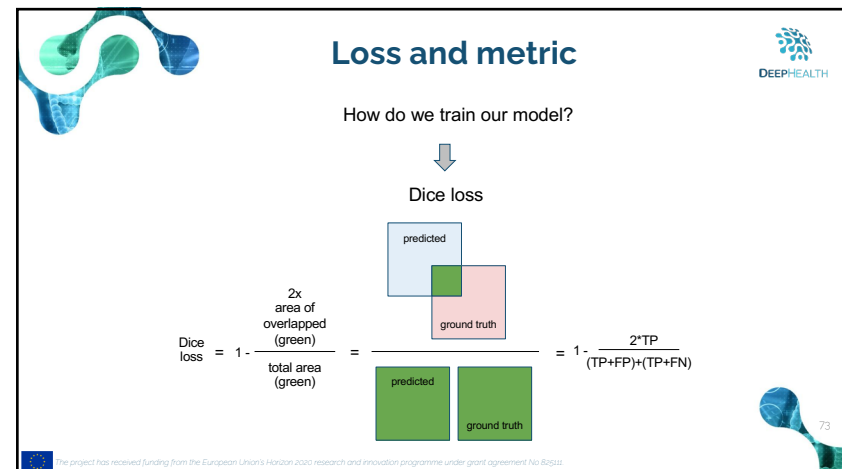
70



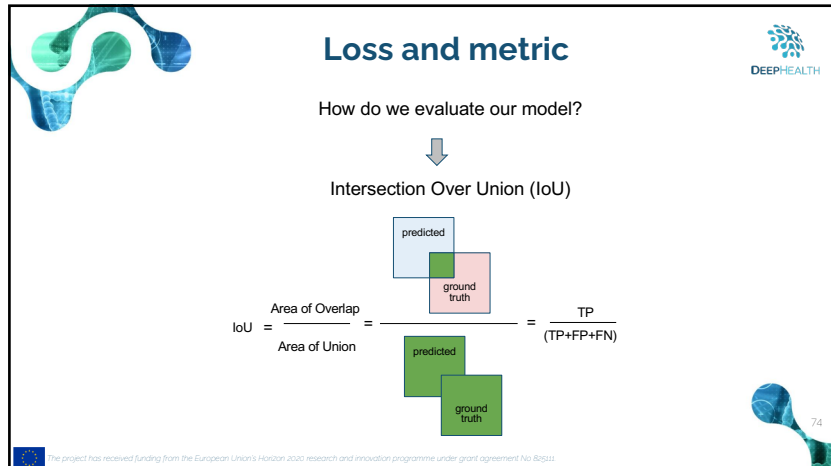
71



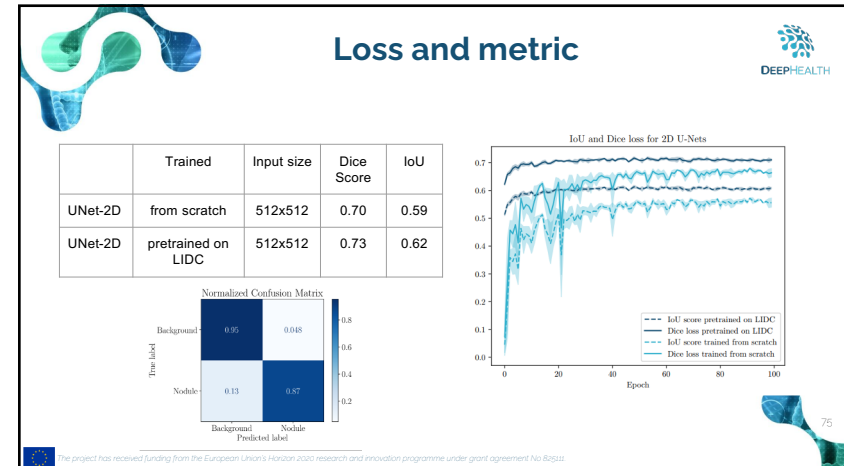
72



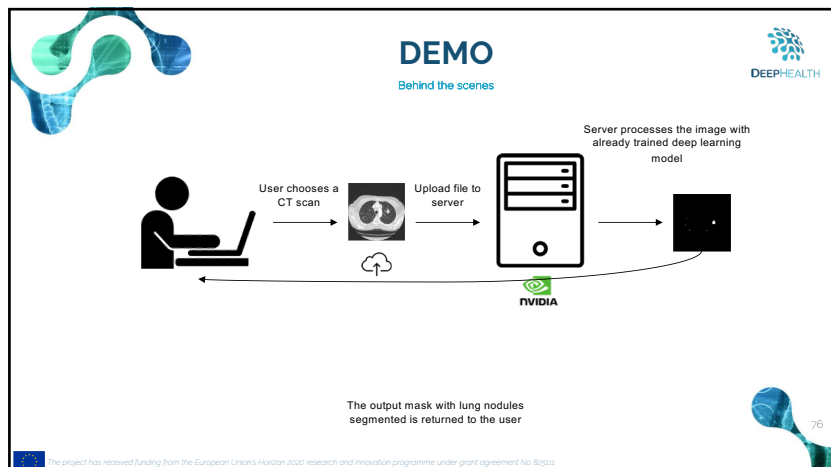
73



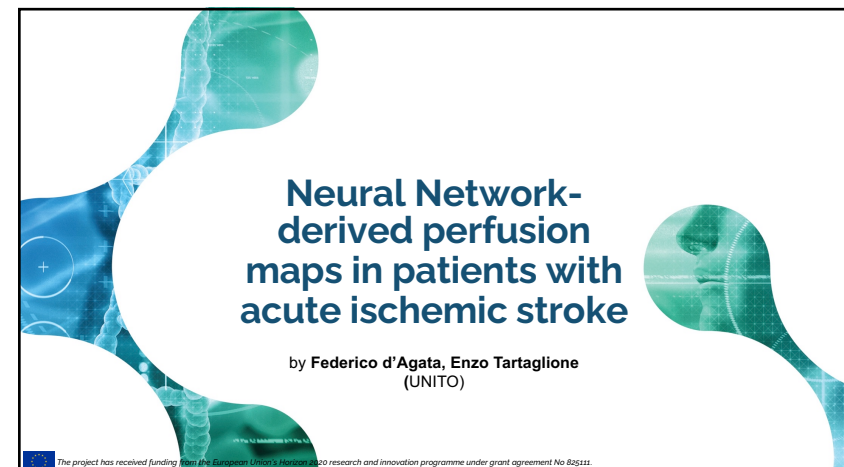
74



75



76



77

**Outline**




• Acute ischemic strokes  
 • What is it possible to do? CT-perfusion  
 • Standard approaches and limits  
 • Deep learning approach and its potential

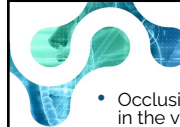
78

The project has received funding from the European Union's Horizon 2020 research and innovation programme under grant agreement No 825111.

DeepHealth Winter School  
24-28 January 2022

78

**Core and Penumbra**




• Occlusion of a cerebral artery causes sudden decrease of the blood perfusion in the vascular territory matching the occluded vessel.  
 • In the ischemic non-functioning area of the brain two different regions may be identified: a central "core", and a peripheral "penumbra", respectively corresponding to areas of irreversible damage and potential recovery.

A. occluded vessel, B. core/penumbra. Collard, Duprez, Jamali S. JBSR 2019;103(1):61.

Sharath Kumar, Chinmay, Nagesh. J Clin Interv Radiol ISVIR 2018;2:155-68

79

The project has received funding from the European Union's Horizon 2020 research and innovation programme under grant agreement No 825111.

DeepHealth Winter School  
24-28 January 2022

79

**CT-perfusion**




• CT perfusion (CTP) protocols are used to sample parenchymal wash-in and wash-out of an iodinated contrast agent in order to assess capillary blood-flow dynamics.  
 • Time-concentration curves are generated for each voxel of the CT images after selection of arterial input and venous output vessels.  
 • Deconvolution-based methods aim to correct for physiologic variability such as arterial delay (i.e. poor cardiac output or carotid stenosis), contrast bolus dispersion (i.e. collateral vessels), and slower injection rates.

Konstas AA, et al. AJNR Am J Neuroradiol 2009;30(4):662-8.  
 Miles KA. Br J Radiol 1991;64(761):409-12.

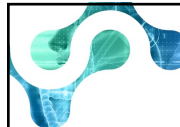
80

The project has received funding from the European Union's Horizon 2020 research and innovation programme under grant agreement No 825111.

DeepHealth Winter School  
24-28 January 2022

80

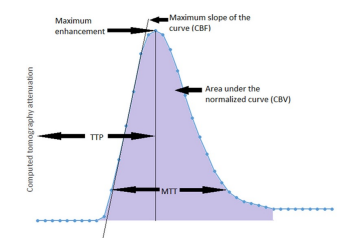
**CT-perfusion**




• An exam to retrieve maps indicating

- Blood Flow (CBF),
- Blood Volume (CBV),
- Mean Transit Time (MTT),
- Time to Peak (TTP).

• A series of low-dose scans are acquired after contrast bolus injection

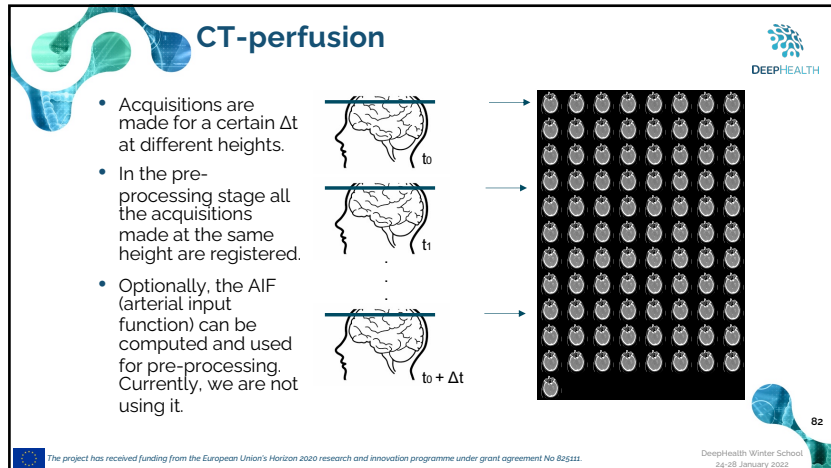


81

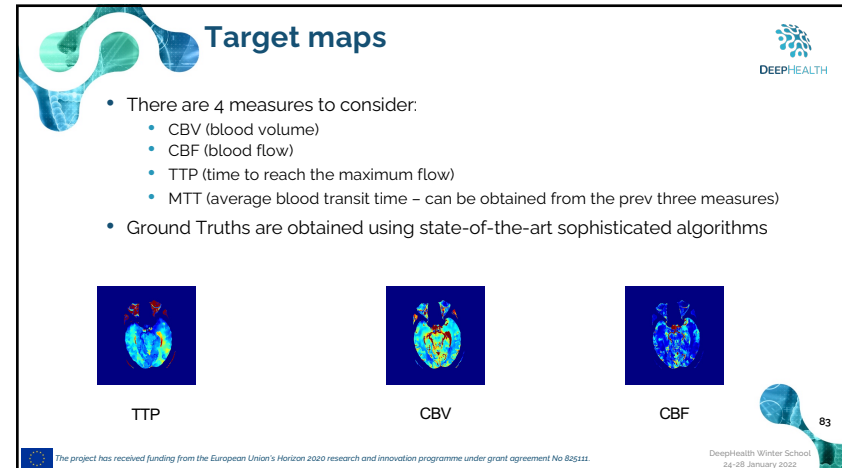
The project has received funding from the European Union's Horizon 2020 research and innovation programme under grant agreement No 825111.

DeepHealth Winter School  
24-28 January 2022

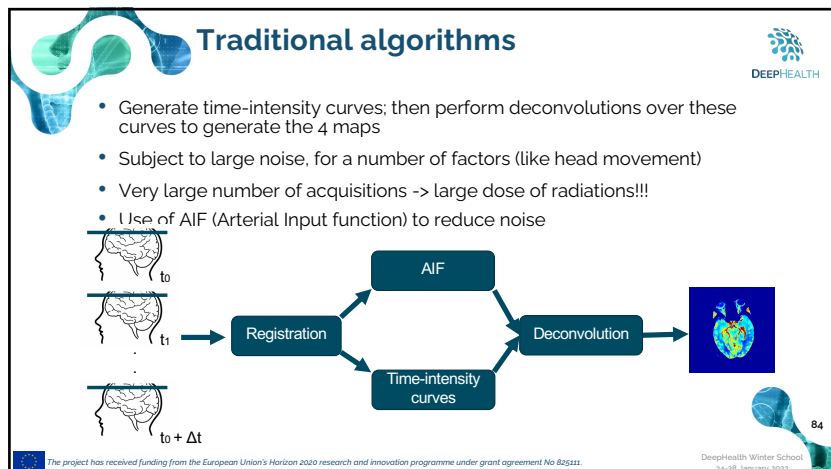
20



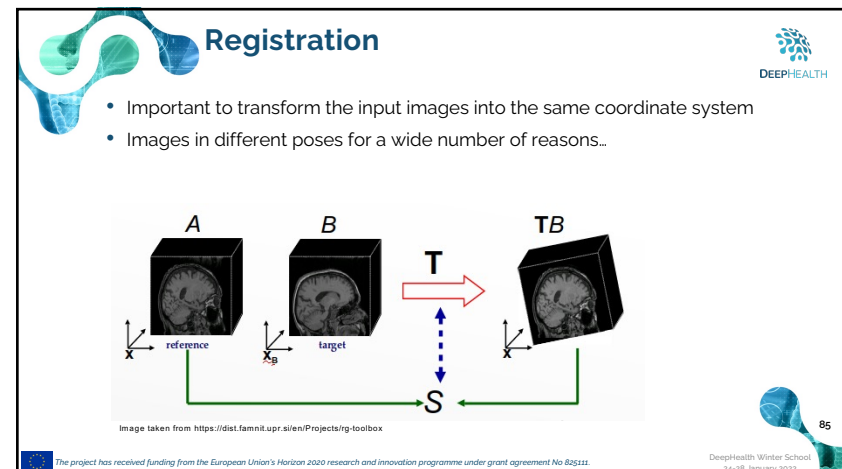
82



83



84



## Arterial Input Function

• AIF describes the concentration of the tracer in blood in an artery.  
 • It is valued over a time scale  
 • It is typically used to evaluate the measures of our interest!

Figure from Perfusion Computed Tomography in Traumatic Brain Injury - Scientific Figure on ResearchGate. Available from: [https://www.researchgate.net/figure/A-An-arterial-input-function-AIF-arrow-on-the-axial-CT-scan-is-used-to-calibrate-the-\\_fig2\\_325059327](https://www.researchgate.net/figure/A-An-arterial-input-function-AIF-arrow-on-the-axial-CT-scan-is-used-to-calibrate-the-_fig2_325059327)

The project has received funding from the European Union's Horizon 2020 research and innovation programme under grant agreement No 825111.

DeepHealth Winter School 24-28 January 2022

86

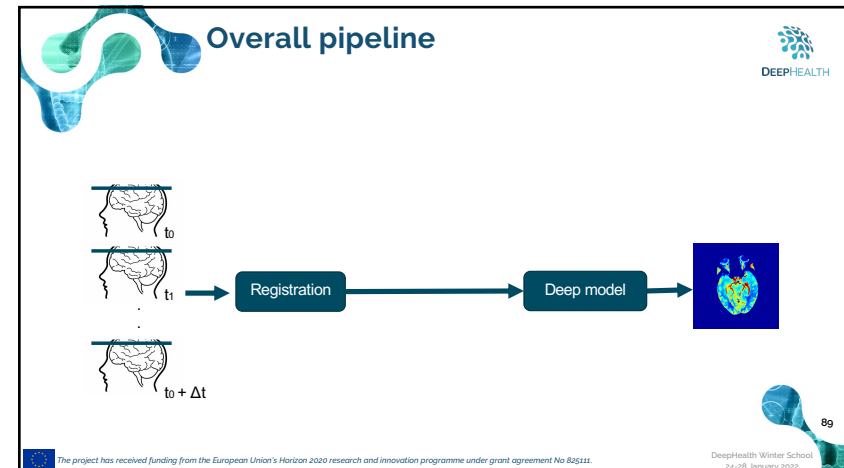
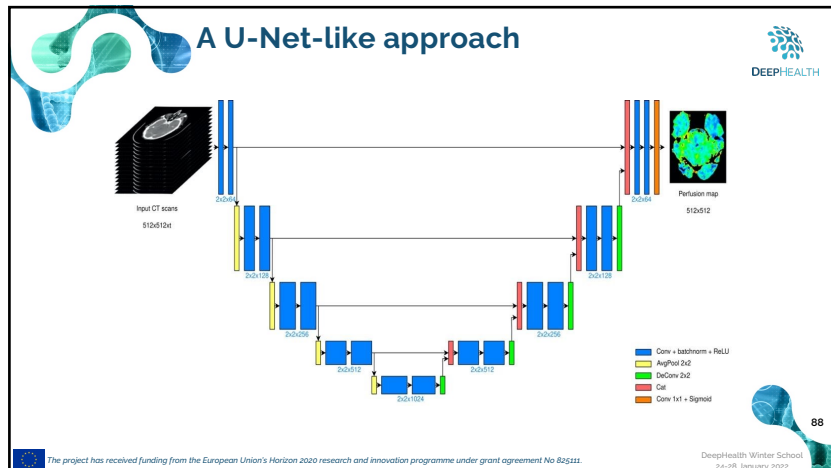
## Why a deep learning approach?

- Possibility to build models robust to noise
- Automatic learning, without imposing strong priors to the preprocessing
- Potentiality to reduce the sampling rate (meaning less radiations!)

The project has received funding from the European Union's Horizon 2020 research and innovation programme under grant agreement No 825111.

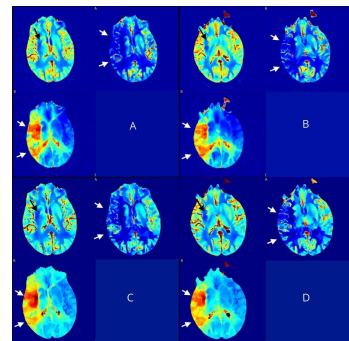
DeepHealth Winter School 24-28 January 2022

87



**Results achieved**  
(Qualitative results using full temporal resolution)

- (A, B) CNN outputs maps from a validation set (CBV, CBF and TTP).
- (C, D) matching sections of GT maps.
- Small infarct core displayed in the CBV map at the right basal ganglia (black arrows)
- Extended penumbra showed in the CBF and TTP maps across right middle cerebral artery territories (white arrows).

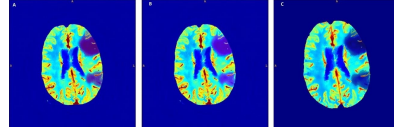


The project has received funding from the European Union's Horizon 2020 research and innovation programme under grant agreement No 825111.  
DeepHealth Winter School  
24-28 January 2022

90

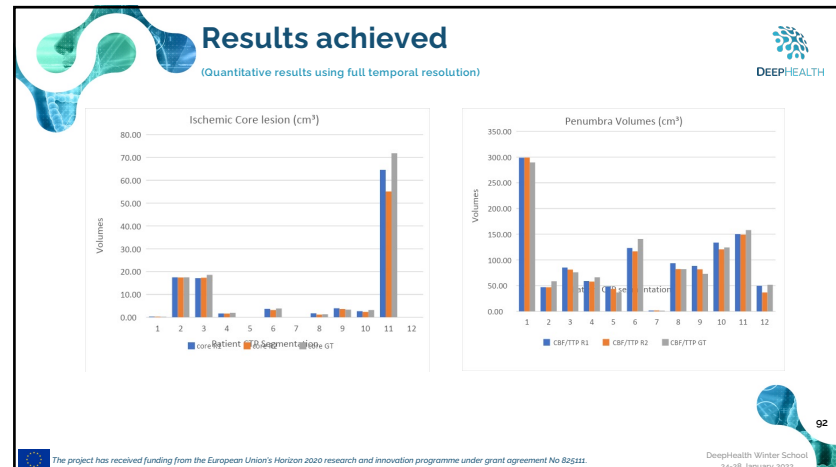
**Results achieved**  
(Qualitative results using full temporal resolution)

- Core segmented on CNN CBV map by rater 1 (A) and rater 2 (B); core segmented on GT map (C).
- The CNN segmented volumes from both raters were matched with the GT to assess overlapping regions by calculating the Dice Similarity Coefficient (DSC).
- DSC > 0.70 in this context is typically considered as good-matching.

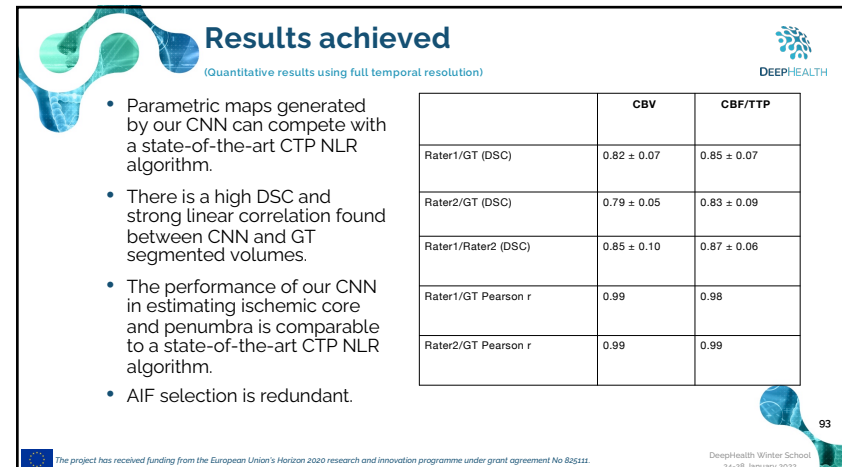


The project has received funding from the European Union's Horizon 2020 research and innovation programme under grant agreement No 825111.  
DeepHealth Winter School  
24-28 January 2022

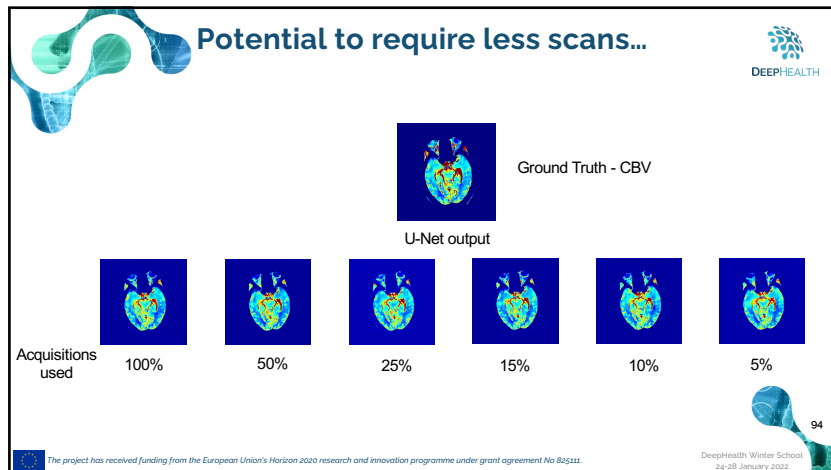
91



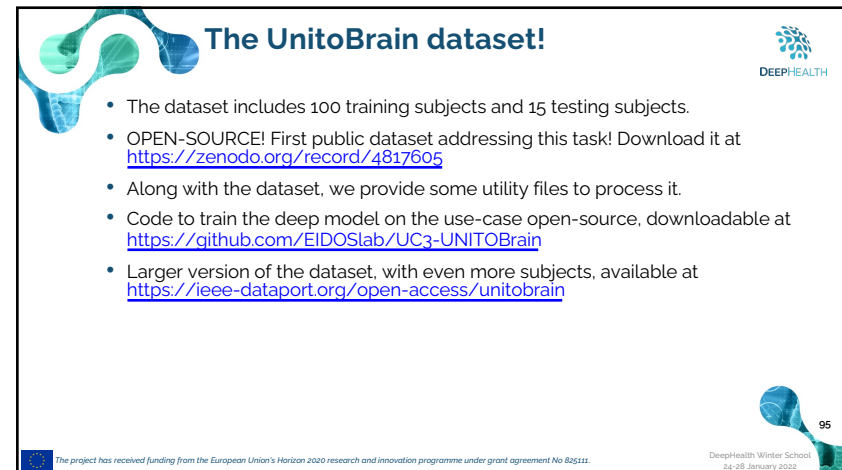
92



93



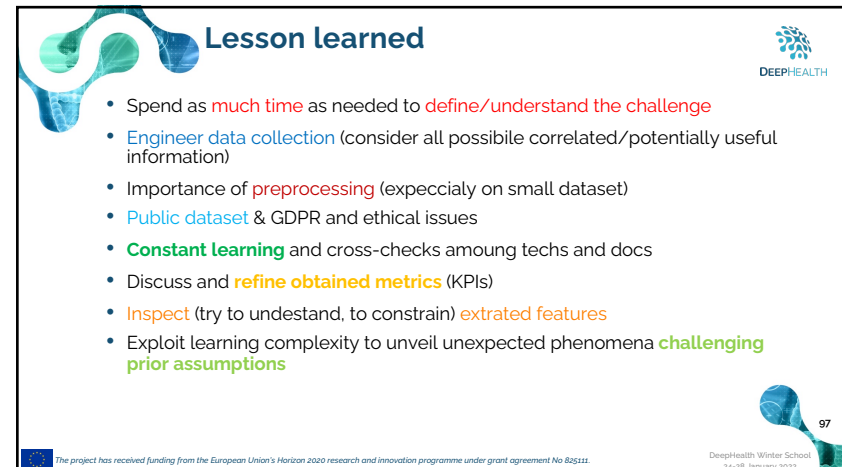
94



95



96



24

